Rest-frame quasistatic theory for rotating electromagnetic systems and circuits

Ben Z. Steinberg ●*

School of Electrical Engineering, Tel-Aviv University, Tel Aviv 69978, Israel

Nader Engheta ●

Department of Electrical and Systems Engineering, University of Pennsylvania, Philadelphia, Pennsylvania 19104, USA

A quasistatic theory for slowly rotating electromagnetic systems observed in their rest frame of reference is developed. Rotation-induced electrodynamic effects are explored, and their electric circuitry implications are discussed. It is shown that rotation may induce fictitious charges that affect lumped device dynamics and offer various device functionalities such as voltage-excited magnetic fields leading to rotation-induced memristors of positive or even negative memristance and their dualities. Rotation-induced electromagnetic gain and instabilities may exist, manifested either as parasitic processes that hamper electric circuitry functionality or as a mean for possible energy harvesting methodology in which the large-scale rotating platform serves as an essentially unlimited energy reservoir. Furthermore, as many artificially engineered electromagnetic materials consist of meta-atoms whose internal dynamics is essentially quasistatic, the study also potentially paves the way for new types of metamaterials. These effects depend on the rotation rate $\mathbf{\Omega}$ but are essentially independent of the axis location. This fundamental property renders them extremely robust and has far-reaching ramifications for a plethora of applications. A preliminary quantitative analysis for $\mathbf{\Omega}$ typical of large-scale platforms ranging from planets to artificial gravity structures is presented.

I. INTRODUCTION

The universal ubiquity of rotation is astounding. It can be observed on nearly any imaginable scale, from multi-kiloparsec galaxies, to planetary systems, to individual planets spinning around their own axis, to man-made structures and machines, down to the microscopic realm. This omnipresence inevitably affects the human experience in general and scientific and technological advances in particular. It is often the case that rotation is experienced or most naturally observed in its rest frame of reference, leading to challenging dynamical problems with intriguing properties. Nonetheless, the study of applied rest-frame electrodynamics (ED) of rotating systems is traditionally motivated mainly by its use in optical gyroscopes for rotation sensing with applications for inertial navigation systems [1–3]. The underlying physics is based on the Sagnac effect [4], in which the phase accumulated by a light signal that propagates along a slowly rotating closed path depends linearly on the path's angular velocity $\mathbf{\Omega}$ and on its enclosed area when observed in the path's rest frame. Recent studies extended the rest-frame ED to wavelength-scale rotating structures, e.g., photonic crystals [5–7], degenerate-mode microcavities [6,8–12], and interference in metamaterials [13], to name a few. Yet these works are almost exclusively limited to the wave optics in which the system dimensions are comparable to or larger than the electromagnetic wavelength. Little attention has been devoted

to studying the rotation footprint in the benign building blocks of technology: electrical devices and circuits operating in the static or deep quasistatic regime.

This lack motivates the present study; our goal is to develop an *ab initio* theory governing the internal ED of electric circuits and systems undergoing rigid slow rotation $\mathbf{\Omega}$, the precise definition of which is provided below. Our interest is focused on observing the ED in $\mathcal{R}^{\Omega}$, the rotating system *rest* frame of reference (FOR). We limit our study to *free* rotations, i.e., rotations not caused by gravitational fields. Thus, it pertains to, e.g., the spinning of a planet around its axis, the spinning of artificial gravity structures [14–16], and more. We exclude rotations of a mass trapped in a gravitational field (e.g., the rotation of Earth around the Sun). While adhering to the slow rotation regime defined below, $\mathbf{\Omega}$ in the aforementioned physical and engineering settings spans many orders of magnitude; Earth and Mars rotate at $\Omega \approx 7.3 \times 10^{-5}$ rad/s, whereas space stations and artificial gravity structures currently under investigation are anticipated to spin at 1–25 rpm, yielding $\Omega \approx 0.1$–2.5 rad/s [14–16]. Rotation-based artificial gravity is given by $\Omega^2 r$, where r is the rotation radius. Thus, in [15,16] effort was devoted to increasing Ω in order to achieve sufficient gravity in smaller structures.

Our study reveals rotation-induced ED effects in $\mathcal{R}^{\Omega}$, such as fictitious electric and magnetic charges leading to different device functionalities, and ED gain and instabilities that may arise in electric circuits, where the rotating platform serves as an essentially unlimited energy reservoir from which the gain mechanism is fed. We also derive a general Poynting theorem in $\mathcal{R}^{\Omega}$, in which an explicit term that formally governs this

*steinber@eng.tau.ac.il

energy exchange is obtained. The effects described above are essentially independent of r or of the location of the rotation axis, scaling only with Ω. This fundamental property renders them extremely robust. Furthermore, it may give rise to a new set of conflicting engineering considerations and compromises, e.g., for an artificial gravity design in which the goal of reducing the structure dimensions implies an increase of Ω. We also note that the rotation-induced ED gain in electric circuits can be regarded not only as a parasitic instability; potentially, it may be used as a means to harvest electromagnetic energy from an already rotating platform without any additional moving parts. The harvesting rate is again independent of the distance from the rotation axis; it is the same whether the system is located at one of the poles or at the equator. These effects are shown to exist already at the level of basic inductor-capacitor elements and circuits. Many modern artificially engineered electromagnetic materials are made of arrays of meta-atoms such as the omega particle and split-ring resonators [17,18], whose internal dynamics is essentially similar to lumped *LC* circuits. Thus, our study may pave the way to new metamaterial functionalities and applications.

It is instructive to point out connections between the present study and seemingly unrelated research endeavors of current interest. The rotation is manifested by the bian-isotropic *r*-dependent constitutive relations in Eqs. (2a) and (2b) below, resembling the Tellegen medium [19] and topological insulators (TIs) [20]. TIs may support an internal fictitious magnetic monopole induced by an external electric charge located near its surface [21]. Our rotation-induced fictitious electric and magnetic charges do not need the presence of a material; the TI role is played here by the rotation itself but in a more complex manner. Along a different track, our rotation-induced fictitious charges suggest a different implementation of memristors [22,23] with positive or negative memristance and their electronic dualities. These connections may inspire and stimulate further advances in their respective fields.

II. FORMULATION

We define $\mathcal{R}_I$ as a static inertial FOR, in which the basic physical laws appear in their simple familiar form. Space-time is flat (gravitation is neglected, and Riemann curvature vanishes); hence, the system geometry is *Lorentzian* [24], and Maxwell's equations (MEs) take on their familiar form in vacuum within the framework of special relativity. A stationary material in $\mathcal{R}_I$ is presented here by the permittivity and permeability scalars $\epsilon(\boldsymbol{r}) = \epsilon_0 \epsilon_r(\boldsymbol{r})$ and $\mu(\boldsymbol{r}) = \mu_0 \mu_r(\boldsymbol{r})$.

We study statics and low-frequency ED in materials and structures that rotate *rigidly* at a constant angular velocity $\boldsymbol{\Omega} = \Omega \hat{\boldsymbol{z}}$ with respect to $\mathcal{R}_I$ around its $\hat{\boldsymbol{z}}$ axis. The spatial extent $D \perp \hat{\boldsymbol{z}}$ occupied by the material is finite and satisfies $\Omega D \ll c$. We focus on the ED as seen by an observer that is *fixed* to the rotating material or structure. Hence, we define the rotating FOR $\mathcal{R}^\Omega$; it is at rest relative to the structure. The $\hat{\boldsymbol{z}}$ axis of $\mathcal{R}^\Omega$ coincides with that of $\mathcal{R}_I$. Here and henceforth, we observe the ED as seen in the FOR $\mathcal{R}^\Omega$, and the corresponding problem is termed the "$\mathcal{R}^\Omega$ problem." The specific case of $\mathcal{R}^0$ and the "$\mathcal{R}^0$ problem" correspond to $\Omega = 0$, meaning the material

and the observer are at rest in the inertial FOR $\mathcal{R}_I$, making $\mathcal{R}^0$ and $\mathcal{R}_I$ identical. $\mathcal{R}^\Omega$ ($\Omega \neq 0$) is noninertial; an observer at rest there sees curved space-time. However, space-time in $\mathcal{R}^\Omega$ can be considered *locally flat* (and Lorentzian) for distances D satisfying [24]

$$D \ll L = c^2/A, \tag{1}$$

where A is the acceleration of $\mathcal{R}^\Omega$ as seen in $\mathcal{R}_I$. Here $A = \Omega^2 D$, so Eq. (1) yields the slow rotation condition mentioned above, $\Omega D \ll c$. Our work is limited to this domain, implying space-time invariance of the (Minkowski) metrics. Then, the covariant formulation of electrodynamics for the $\mathcal{R}^\Omega$ problem is given by the same set of MEs as for the $\mathcal{R}^0$ problem but with modified constitutive relations to account for rotation [25,26],

$$\boldsymbol{B} = \mu \boldsymbol{H} + c^{-2}(\boldsymbol{\Omega} \times \boldsymbol{r}) \times \boldsymbol{E}, \tag{2a}$$

$$\boldsymbol{D} = \epsilon \boldsymbol{E} - c^{-2}(\boldsymbol{\Omega} \times \boldsymbol{r}) \times \boldsymbol{H}, \tag{2b}$$

where ϵ and μ are the material properties and $c = (\mu_0 \epsilon_0)^{-1/2}$ is the speed of light in *vacuum*, all of which as apply for the $\mathcal{R}^0$ problem. Note that the rotation-induced term in the constitutive relations is independent of the material properties. Here and henceforth, vectors are written in bold letters, and a hat indicates a unit vector. In $\mathcal{R}^\Omega$ the coordinates normal to the rotation axis are denoted by $\boldsymbol{\rho} = \hat{\boldsymbol{x}} x + \hat{\boldsymbol{y}} y = \rho \hat{\boldsymbol{\rho}}$. Thus, $\boldsymbol{\Omega} \times \boldsymbol{r} = \Omega \rho \hat{\boldsymbol{\varphi}}$, where $\hat{\boldsymbol{\varphi}}$ is the azimuthal direction.

A. Poynting theorem in $\mathcal{R}^\Omega$

The condition in Eq. (1) and the ensuing metric invariance imply space-time invariance of the momentum-energy tensor. Consequently, the Poynting vector $\mathbb{S} = \mathbb{E} \times \mathbb{H}$, where $\mathbb{E}$ and $\mathbb{H}$ are the full time-dependent fields, has the same physical meaning for power flow density, whether we are dealing with the $\mathcal{R}^0$ or $\mathcal{R}^\Omega$ problem. Likewise, $\mathbb{E} \cdot \mathbb{J}$ preserves its meaning as well as other quantities in the theorem. Using the standard derivation and some vector manipulations, we arrive at the Poynting theorem for $\mathcal{R}^\Omega$ problems (see the Supplemental Material [27]),

$$-\boldsymbol{\nabla} \cdot \mathbb{S} = \mathbb{E} \cdot \frac{\partial}{\partial t}(\epsilon \star \mathbb{E}) + \mathbb{H} \cdot \frac{\partial}{\partial t}(\mu \star \mathbb{H}) + \mathbb{E} \cdot \mathbb{J}$$
$$+ \frac{2}{c^2} \rho \dot{\Omega} \hat{\boldsymbol{\varphi}} \cdot \mathbb{S} + \frac{1}{c^2} \rho \Omega \hat{\boldsymbol{\varphi}} \cdot \dot{\mathbb{S}}, \tag{3}$$

where the overdot represents the time derivative and the star ($\star$) represents simple multiplication and time convolution for the nondispersive and dispersive media, respectively. The two new terms on the right-hand side represent the power exchange between the electromagnetic (EM) fields and the rotation energy. This exchange is possible only where $\mathbb{S}$ is not normal to the rotation direction $\hat{\boldsymbol{\varphi}}$. Usually, the rotation energy can be considered to be essentially infinitely large compared to the EM one; hence, it is hardly depleted (or, alternatively, kept constant by external independent mechanical means), and one can assume $\dot{\Omega} = 0$.

B. Boundary conditions in $\mathcal{R}^\Omega$

The field's continuity or boundary conditions follow directly from the MEs. Since the structure of the latter is the same as that for a $\mathcal{R}^0$ problem, the boundary conditions

written on tangential E and H and normal D and B are, in principle, unchanged. However, it is instructive to examine the implied conditions on the normal E and H, as they will be used later. They are given by (see the Supplemental Material [27])

$$\hat{\boldsymbol{n}} \cdot (\epsilon_1 \boldsymbol{E}_1 - \epsilon_2 \boldsymbol{E}_2) = \eta_{ef} - c^{-2}\Omega\rho\hat{\boldsymbol{\varphi}} \cdot \boldsymbol{K}_{ef}, \quad (4a)$$

$$\hat{\boldsymbol{n}} \cdot (\mu_1 \boldsymbol{H}_1 - \mu_2 \boldsymbol{H}_2) = 0, \quad (4b)$$

where $\boldsymbol{K}_{ef}$ is the surface density of the free electric current. This last result tells us that $\hat{\boldsymbol{n}} \cdot \mu\boldsymbol{H}$ should pass continuously just like $\hat{\boldsymbol{n}} \cdot \boldsymbol{B}$, despite the additional rotation-induced term in the constitutive relation for $\boldsymbol{B}$.

C. Statics in $\mathcal{R}^\Omega$

Similar to quasistatic theory for $\mathcal{R}^0$ problems, the static fields in $\mathcal{R}^\Omega$ constitute the leading terms in the slowly time varying quasistatic electrodynamics of $\mathcal{R}^\Omega$ problems. Thus, we set $\frac{\partial}{\partial t} \equiv 0$ in $\mathcal{R}^\Omega$ and assume that our domain is simply connected with no electric current. Then we may still define

$$\boldsymbol{E} = -\nabla\Phi_e, \quad \boldsymbol{H} = -\nabla\Phi_m. \quad (5)$$

We now use these expressions in the time-independent Maxwell equations in $\mathcal{R}^\Omega$ and the constitutive relations in Eqs. (2a) and (2b). With no further assumptions or approximations we obtain the following exact equations governing the static fields (see Sec. I in the Supplemental Material [27]):

$$\nabla \cdot \epsilon \nabla\Phi_e = -\rho_{ef} + \frac{2\Omega}{c^2}\frac{\partial}{\partial z}\Phi_m, \quad (6a)$$

$$\nabla \cdot \mu \nabla\Phi_m = -\frac{2\Omega}{c^2}\frac{\partial}{\partial z}\Phi_e, \quad (6b)$$

where ρ_{ef} is the free *real* electric charge density. These equations possess several interesting properties.

(i) The formulation and hence the field solutions are *independent of the location of the rotation axis*. The only footprint of the rotation axis is its direction $\hat{\boldsymbol{z}}$, manifested via the z derivative on the right-hand side. The axis location may sometimes lurk in only through the boundary conditions in Eq. (4a).

(ii) The set has the form of a static $\mathcal{R}^0$ problem, where the rotation manifests via fictitious sources on the right-hand side of the equations above; the fictitious electric source is $\rho_e = 2\Omega c^{-2}H_z$, while the *fictitious magnetic source* is $\rho_m = -2\Omega c^{-2}E_z$. Note, however, that this is a source for $\mu\boldsymbol{H}$, as implied by Eq. (6b): $\nabla \cdot \mu\boldsymbol{H} = -2\Omega c^{-2}E_z$. We still have $\nabla \cdot \boldsymbol{B} = 0$, as we should since there is no real magnetic charge.

One fundamental result of the coupled equations above is the fact that unlike statics in $\mathcal{R}^0$ problems, here boundary conditions for E and H cannot be set independently; imposing boundary conditions on, e.g., Φ_e affects H at the boundary. To illustrate this, we consider the high electric conductor (HEC) in which the conductivity is very high (but not infinite). The electric field in this material is effectively zero. From Eq. (5), this implies $\Phi_e = $ const in the HEC and on its boundary. Consider now the schematic example in Fig. 1 consisting of two HEC plates with potential difference $V = \Phi_{e2} - \Phi_{e1}$. We show below that up to first order in Ω, E is the same as in the corresponding $\mathcal{R}^0$ problem, namely, $\boldsymbol{E} = \hat{\boldsymbol{z}}E_z = -\hat{\boldsymbol{z}}V/d$ (neglecting the edge effects), as seen in Fig. 1(a). Thus, a rotation-induced fictitious magnetic charge $\rho_m = 2\Omega c^{-2}V/d$

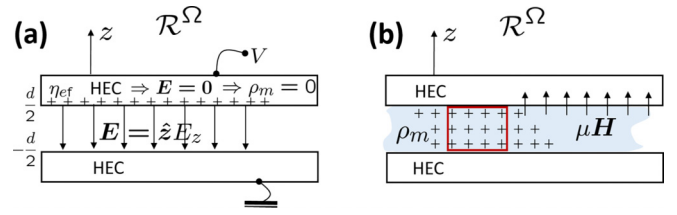FIG. 1. Penetration of rotation-induced magnetic field into a HEC in $\mathcal{R}^\Omega$. (a) An electric field normal to the surface exists, e.g., in a capacitor. (b) The $\hat{\boldsymbol{z}}$ component of this field generates the fictitious magnetic charge ρ_m between the plates. Inside the HEC material $\boldsymbol{E} = \boldsymbol{0}$; hence, $\rho_m = 0$ there. The application of Gauss's theorem for $\mu\boldsymbol{H}$ in $\mathcal{R}^\Omega$ to the square volume and the continuity condition in Eq. (4b) yield a magnetic field normal to the surface that penetrates the HEC.

is generated in the space between the plates. Since $\boldsymbol{E} = \boldsymbol{0}$ inside the HEC, no ρ_m exists there. By applying Gauss's law for $\mu\boldsymbol{H}$, say, in the red rectangular volume in Fig. 1(b), it is seen that normal $\mu\boldsymbol{H}$ must exist on the HEC surface, and it penetrates the plates by virtue of the continuity requirement in Eq. (4b). This field is first order in Ω and independent of the distance from the rotation axis. Thus, rotation-induced magnetic fields in $\mathcal{R}^\Omega$ may possess a normal component at a HEC surface and may penetrate it. This is reminiscent of the magnetic field dynamics in HECs and superconductors. While the latter are known to repel magnetic fields, a phenomenon known as the Meissner effect [28], a rotating superconductor supports normal magnetic fields penetrating through its surface, a phenomenon known as the London moment that has been studied theoretically [28,29] and experimentally [30].

The above holds for *statics* in $\mathcal{R}^\Omega$. For slow time variation at the frequency ω for which the quasistatic regime applies, the solutions of Eqs. (6a) and (6b) constitute the *leading term* of a quasistatic power series in ω (see examples below and in Sec. 4 in the Supplemental Material [27]). Then the EM fields penetrate HEC with conductivity σ up to the skin depth $\delta = \sqrt{2/(\omega\mu\sigma)}$. Thus, for HEC of thickness $T = a\delta$, $a \leqslant 1$, the normal H penetrates and passes continuously through the HEC, whose effective resistance per unit length is $R \propto (\sigma T)^{-1} = a^{-1}\sqrt{\omega\mu/(2\sigma)}$. Consequently, R can be made as small as one wishes (e.g., by tuning ω), while still the normal H passes through the thin HEC continuously. This parametric regime is implicitly assumed below.

D. Power series in Ω for static fields

Solutions to the coupled equations (6a) and (6b) are difficult to derive even for simple geometries. Great simplification is achieved by applying the solution technique of power series in Ω. This approach is also motivated by the fact that under the slow rotation condition $\Omega D/c$ is a small parameter; thus, excellent approximations can be obtained by keeping only a very small number of leading terms (say, only zeroth and first order). More precisely, let $\ell \leqslant D$ be the typical length scale on which Φ_e and Φ_m vary. The right-hand sides of Eqs. (6a) and (6b) are much smaller than the left-hand sides if $\Omega n\ell/c \ll 1$ ($n^2 = \mu\epsilon c^2$). Below we limit ourselves to this condition, which is easily met in practice. This procedure can

then serve as a starting point for a study that incorporates both rotation at angular frequency Ω and quasistatic time variation of the field at frequency ω.

We express Φ_e and Φ_m as

$$\Phi_e(\boldsymbol{r}) = \sum_{n=0}^{\infty} \Omega^n \Phi_e^{(n)}(\boldsymbol{r}) \Rightarrow \boldsymbol{E} = \sum_{n=0}^{\infty} \Omega^n \boldsymbol{E}^{(n)}(\boldsymbol{r}), \qquad (7\text{a})$$

$$\Phi_m(\boldsymbol{r}) = \sum_{n=0}^{\infty} \Omega^n \Phi_m^{(n)}(\boldsymbol{r}) \Rightarrow \boldsymbol{H} = \sum_{n=0}^{\infty} \Omega^n \boldsymbol{H}^{(n)}(\boldsymbol{r}), \qquad (7\text{b})$$

where $\boldsymbol{E}^{(n)}(\boldsymbol{r}) = -\nabla \Phi_e^{(n)}(\boldsymbol{r})$ and $\boldsymbol{H}^{(n)}(\boldsymbol{r}) = -\nabla \Phi_m^{(n)}(\boldsymbol{r})$. Substituting these series into Eqs. (6a) and (6b) and equating similar powers of Ω, we obtain

$$\nabla \cdot \epsilon \nabla \Phi_e^{(0)} = -\rho_{ef}, \quad \nabla \cdot \mu \nabla \Phi_m^{(0)} = 0 \qquad (8\text{a})$$

for the leading terms and

$$\nabla \cdot \epsilon \nabla \Phi_e^{(n)} = \frac{2}{c^2} \frac{\partial}{\partial z} \Phi_m^{(n-1)} \quad \left(= -\rho_e^{(n)}\right), \qquad (8\text{b})$$

$$\nabla \cdot \mu \nabla \Phi_m^{(n)} = -\frac{2}{c^2} \frac{\partial}{\partial z} \Phi_e^{(n-1)} \quad \left(= -\rho_m^{(n)}\right) \qquad (8\text{c})$$

for the higher-order terms $n = 1, 2, \ldots$. The leading terms $\Phi_e^{(0)}$ and $\Phi_m^{(0)}$ are nothing but the solutions of the corresponding $\mathcal{R}^0$ problem. They "excite" the higher-order terms that represent the Ω-dependent effects. The $\boldsymbol{D}$ and $\boldsymbol{B}$ power series are given by

$$\boldsymbol{D} = \sum_{n=0}^{\infty} \Omega^n \boldsymbol{D}^{(n)}, \quad \boldsymbol{D}^{(n)} = \epsilon \boldsymbol{E}^{(n)} - \frac{1}{c^2} \rho \hat{\boldsymbol{\varphi}} \times \boldsymbol{H}^{(n-1)}, \qquad (9\text{a})$$

$$\boldsymbol{B} = \sum_{n=0}^{\infty} \Omega^n \boldsymbol{B}^{(n)}, \quad \boldsymbol{B}^{(n)} = \mu \boldsymbol{H}^{(n)} + \frac{1}{c^2} \rho \hat{\boldsymbol{\varphi}} \times \boldsymbol{E}^{(n-1)}, \qquad (9\text{b})$$

with $\boldsymbol{D}^{(0)} = \epsilon \boldsymbol{E}^{(0)}$ and $\boldsymbol{B}^{(0)} = \mu \boldsymbol{H}^{(0)}$. The nth-order term $\boldsymbol{D}^{(n)}$ incorporates $\boldsymbol{E}^{(n)}$ and $\boldsymbol{H}^{(n-1)}$. The structure of $\boldsymbol{B}^{(n)}$ is similar.

Note that we keep the physical units of Ω. Thus, the units of, e.g., $\boldsymbol{E}^{(n)}$ are $(\text{s})^n \times \text{V/m}$. This could be avoided by using a normalized dimensionless rotation rate $\bar{\Omega} = \Omega \ell / c$ that may be preferable from the formal mathematical viewpoint. However, such normalization necessarily reintroduces ℓ into the equations (with respect to which $\boldsymbol{r}$ can be normalized), rendering the ensuing physical examples less transparent. Thus, we choose to keep the physical units and implicitly assume that $\Omega n \ell / c \ll 1$ holds. A similar approach is used in many classical power-series analyses of physical problems; a celebrated example is the Luneburg-Kline power series of $1/k_0$ that lays the foundation of geometrical optics [31].

E. Rotation footprint on self-capacitance and inductance

From Gauss's law the free real electric charge on the capacitor plates is $\eta_{ef} = \hat{\boldsymbol{n}} \cdot (\boldsymbol{D_1} - \boldsymbol{D_2})$, yielding

$$\eta_{ef} = \hat{\boldsymbol{n}} \cdot (\epsilon_1 \boldsymbol{E}_1 - \epsilon_2 \boldsymbol{E}_2) - \frac{\Omega \rho}{c^2} \hat{\boldsymbol{n}} \cdot [\varphi \times (\boldsymbol{H}_1 - \boldsymbol{H}_2)]. \qquad (10)$$

From Eqs. (8a)–(8c) the leading terms of the capacitor fields are $\boldsymbol{E}^{(0)} + O(\Omega^2)$ and $\boldsymbol{H} = \Omega \boldsymbol{H}^{(1)} + O(\Omega^3)$, where $\boldsymbol{E}^{(0)}$ is merely the capacitor field in the $\mathcal{R}^0$ problem. Thus, the rotation footprint on η_{ef} and on the capacitor voltage is only
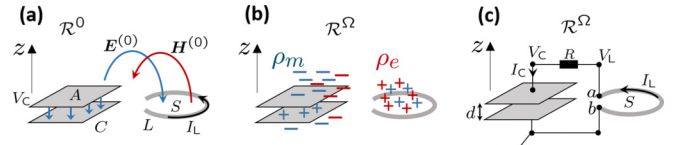

FIG. 2. The ED of the $\mathcal{R}^\Omega$ problem of the *LC* circuit. (a) The zeroth-order fields $\boldsymbol{E}^{(0)}$ (blue) and $\boldsymbol{H}^{(0)}$ (red) are obtained from the corresponding $\mathcal{R}^0$ problem. (b) $\hat{z} \cdot \boldsymbol{E}^{(0)}$ and $\hat{z} \cdot \boldsymbol{H}^{(0)}$ generate rotation-induced fictitious magnetic charge ρ_m (blue) and electric charge ρ_e (red), respectively. (c) The $\mathcal{R}^\Omega$ LC circuit. Connection polarity $\sigma = 1$ ($\sigma = -1$) for loop points a and b (b and a) connected to the upper and lower capacitor plates, respectively.

second order in Ω. As a result, its effect on the capacitance is also of $O(\Omega^2)$. Similar considerations apply to inductors.

III. EXAMPLES

A. LC circuit dynamics

Consider the circuit in Fig. 2. It consists of a parallel plate capacitor C with capacitance C and a loop inductor L with inductance L. From Sec. II E, the effect of Ω on L and C is only of $O(\Omega^2)$; thus, these *intrinsic* properties are practically unchanged. However, rotation-induced L-C intercoupling may give rise to an $O(\Omega)$ footprint on the circuit dynamics.

We assume that the plates and the loop areas A and S are normal to $\hat{z}$, but not necessarily at the same height z. The leading terms of the static solution are obtained from the corresponding $\mathcal{R}^0$ problem; they are the capacitor E field $\boldsymbol{E}^{(0)}$ and inductor H field $\boldsymbol{H}^{(0)}$ shown in Fig. 2(a). They are proportional to the capacitor voltage V_C and inductor current I_L, respectively, expressed conveniently as

$$\boldsymbol{E}^{(0)} = V_C \boldsymbol{f}_e(\boldsymbol{r}), \quad \boldsymbol{H}^{(0)} = I_L \boldsymbol{f}_h(\boldsymbol{r}), \qquad (11)$$

where $\boldsymbol{f}_{e,h}$ are normalized real field patterns. Both C and L may possess external leakage fields of essentially a dipole form [17] but may assume a more complex structure near their respective devices. These leakage fields are included in $\boldsymbol{E}^{(0)}$ and $\boldsymbol{H}^{(0)}$. From Eqs. (8a)–(8c) the first-order rotation-induced fictitious magnetic and electric charges are $\Omega \rho_m^{(1)} = -2\Omega c^{-2} \hat{z} \cdot \boldsymbol{E}^{(0)}$ and $\Omega \rho_e^{(1)} = 2\Omega c^{-2} \hat{z} \cdot \boldsymbol{H}^{(0)}$, respectively, shown in Fig. 2(b). $\rho_m^{(1)}$ ($\rho_e^{(1)}$) resides inside the capacitor (inductor) but may exist also in the external domain due to leakage fields. A blowout of the internal $\rho_m^{(1)}$ is shown in Fig. 1(b). $\rho_m^{(1)}$ and $\rho_e^{(1)}$ are the sources in Eqs. (8b)–(8c) and excite the z-directed first-order electric and magnetic fields,

$$H_z^{(1)}(\boldsymbol{r}) = -\partial_z \Phi_m^{(1)} = V_C \frac{2}{\mu c^2} F_e(\boldsymbol{r}), \qquad (12\text{a})$$

$$E_z^{(1)}(\boldsymbol{r}) = -\partial_z \Phi_e^{(1)} = -I_L \frac{2}{\epsilon c^2} F_h(\boldsymbol{r}), \qquad (12\text{b})$$

where

$$F_{e,h}(\boldsymbol{r}) = \int \partial_z G(\boldsymbol{r}, \boldsymbol{r}') \hat{z} \cdot \boldsymbol{f}_{e,h}(\boldsymbol{r}') \, dv' \qquad (12\text{c})$$

and $G(\boldsymbol{r}, \boldsymbol{r}') = (4\pi |\boldsymbol{r} - \boldsymbol{r}'|)^{-1}$ is the Poisson equation Green's function. The integration extends over the domain where $\rho_m^{(1)}$ and $\rho_e^{(1)}$ (or $E_z^{(0)}$ and $H_z^{(0)}$) do not vanish. From Eq. (12a) the capacitor E field creates a $\hat{z}$-directed magnetic flux $\beta^{(1)}$

through the loop area S,

$$\beta^{(1)} = \int_S B_z^{(1)}(\boldsymbol{r})ds = \mu H_z^{(1)}(\boldsymbol{r}_\mathrm{L})S = V_C \frac{2}{c^2} F_e(\boldsymbol{r}_\mathrm{L})S, \quad (13)$$

where $\boldsymbol{r}_\mathrm{L}$ is the loop center and we assume that $H_z^{(1)}$ is uniform. In the above we used Eq. (9b). Note that since $\boldsymbol{E}^{(0)}$ possesses only a $\hat{z}$ component at $\boldsymbol{r}_\mathrm{L}$ the second term in Eq. (9b) does not contribute to the flux crossing S. $\beta^{(1)}$ in Eq. (13) adds up to the flux created by the intrinsic properties of the loop $\beta^{(0)} = LI_\mathrm{L}$, creating the total flux $\beta = \beta^{(0)} + \Omega\beta^{(1)}$,

$$\beta = LI_\mathrm{L} + V_C \frac{2\Omega}{c^2} F_e(\boldsymbol{r}_\mathrm{L})S. \quad (14)$$

Likewise, the contribution of the rotation-induced electric field $E_z^{(1)}$ in Eq. (12b) to the voltage on the capacitor plates is essentially $E_z^{(1)}d$. Thus, the total voltage developing on C is

$$V_\mathrm{C} = \frac{Q}{C} + I_\mathrm{L} \frac{2\Omega}{\epsilon c^2} F_h(\boldsymbol{r}_\mathrm{C})d, \quad (15)$$

where Q and $\boldsymbol{r}_\mathrm{C}$ are the capacitor charge and center and we assume uniform $E_z^{(1)}$. We now follow the standard procedure of quasistatics for $\mathcal{R}^0$ problems. We assume that the leading terms of the $\mathcal{R}^\Omega$ problem vary slowly in time, with $e^{-i\omega t}$ being the time dependence. A formal double power-series expansion in both frequencies ($\omega^m\Omega^n$) on which this approach is based is provided in the last section of the Supplemental Material [27]. The results presented so far are nothing but the $m = 0, n = 0, 1$ terms. The dynamics of the $m = 1, n = 0, 1$ terms is similar to the first term in conventional quasistatic systems. Thus, the inductor and capacitor voltages V_L and V_C are [using Eq. (15) with $I_\mathrm{C} = -i\omega Q$]

$$V_\mathrm{L} = i\omega\beta, \quad V_\mathrm{C} = i\frac{I_\mathrm{C}}{\omega C} + I_\mathrm{L} \frac{2\Omega}{\epsilon c^2} F_h(\boldsymbol{r}_\mathrm{C})d. \quad (16)$$

If L and C are connected as shown in Fig. 2(c), then $V_\mathrm{L} = \sigma V_\mathrm{C} + RI_\mathrm{L}$, and $I_\mathrm{L} = \sigma I_\mathrm{C}$, where $\sigma = \pm 1$ is the connection polarity and R represents dissipation. Solving Eqs. (14)–(16) for I_L, we obtain

$$\left[\frac{\omega^2}{\omega_0^2} + i\omega\tau - \left(\sigma - i\omega \frac{2\Omega}{c^2} F_h(\boldsymbol{r}_\mathrm{C})A \right) \right.$$
$$\left. \times \left(\sigma - i\omega \frac{2\Omega}{c^2} F_e(\boldsymbol{r}_\mathrm{L})S \right) \right] I_\mathrm{L} = 0, \quad (17)$$

where $\omega_0 = (LC)^{-1/2}$ is the resonance frequency of the corresponding $\mathcal{R}^0$ problem, $\tau = RC$ is the loss parameter, and $A = Cd/\epsilon$ is the capacitor effective area (uniform ϵ is assumed for simplicity). A nontrivial I_L exists at the eigenfrequencies $\omega_{1,2}(\Omega)$ that nullify the polynomial multiplying I_L,

$$\omega_{1,2}(\Omega) = \pm\omega_0 \sqrt{1 - \omega_0^2\tau\left(\sigma\Omega F + \frac{\tau}{4}\right)} - i\omega_0^2\left(\sigma\Omega F + \frac{\tau}{2}\right), \quad (18)$$

where $F = [F_h(\boldsymbol{r}_\mathrm{C})A + F_e(\boldsymbol{r}_\mathrm{L})S]/c^2$ and we kept terms only up to first order in Ω (inclusive). Depending on the connection polarity σ and rotation direction, the eigenfrequency has positive or negative imaginary parts. Recall the $e^{-i\omega t}$ time dependence. If $\sigma\Omega F < 0 \, (>0)$ rotation-induced gain (loss) is present. This gain (loss) is due to the power exchange between

the EM energy stored in the circuit and the mechanical energy stored in the structure rotation. If the gain is sufficiently large to offset dissipation, i.e., $\delta = -\sigma\Omega F - \tau/2 > 0$, net gain exists, and I_L increases exponentially. Note the ω_0^2 multiplication; δ does not need to be large to produce observable gain.

A comment on radiation loss is in order. Accelerating charge always radiates [32]; thus, power loss P_r due to radiation exists even in systems operating in the deep quasistatic regime. This loss effect can be represented in the system by adding a resistor with the appropriate radiation resistance $R_r \propto P_r$, a well-established practice in antenna theory [33]. Then, we have $R = R_L + R_r$, where R_L represents the circuit Ohmic loss. R_r sets a lower bound on R, and hence on τ, that holds even if the system is made of a superconductor with zero Ohmic loss (unless encapsulated in a cavity with superconducting walls). An analytic estimate of R_r is provided in the Supplemental Material [27]. This estimate is used in the numerical calculations in Sec. III B 4.

It may be difficult to evaluate $\mathrm{Im}\{\omega_{1,2}\}$ for general elements. In the following sections we zoom in and study the internal and external near fields of the idealized capacitor and inductor in $\mathcal{R}^\Omega$. This study reveals different functionalities of lumped devices in $\mathcal{R}^\Omega$ and also enables us to engineer different elements for which gain estimates can be obtained.

B. Local fields of lumped devices

The examples in Secs. III B 1, III B 2, and III B 3 consist of truncated idealized structures in which edge effects are ignored. They may represent idealized canonical models for the unintended rotation-induced effect encountered in arbitrary electrical circuits or deliberately designed ones aimed at exploiting these effects. The example in Sec. III B 4 consists of a finite-size structure designed *a priori* to exploit the rotation-induced effects, and furthermore, it allows for exact calculation of the leading fields.

1. Parallel plate capacitor

Consider the structure in Fig. 1. Neglecting edge effects, $\boldsymbol{E}^{(0)} = -\hat{z}V/d$ between the plates, and it vanishes outside the capacitor. Clearly, $\boldsymbol{H}^{(0)} = \boldsymbol{0}$, and $\boldsymbol{B}^{(0)} = \boldsymbol{0}$. However, from Eq. (8c) the fictitious magnetic charge density of $\rho_m = \Omega\rho_m^{(1)} = 2\Omega V/(dc^2)$ exists in the capacitor volume. A straightforward calculation gives for $\boldsymbol{H}^{(1)}$ (see the Supplemental Material [27])

$$\boldsymbol{H}^{(1)} = \hat{z}V \begin{cases} \frac{2z}{\mu dc^2}, & |z| \leqslant d/2, \\ \frac{\pm 1}{\mu c^2}, & z \gtrless \pm d/2. \end{cases} \quad (19a)$$

$\boldsymbol{H}^{(1)}$ increases linearly between the plates and is uniform outside, pointing upward (downward) for $z \gtrless 0$. It is independent of the rotation axis location. With Eq. (9b) we have

$$\boldsymbol{B}^{(1)} = V \begin{cases} \hat{z}\frac{2z}{dc^2} - \hat{\rho}\frac{\rho}{dc^2}, & |z| \leqslant d/2, \\ \pm\hat{z}c^{-2}, & z \gtrless \pm d/2. \end{cases} \quad (19b)$$

Interestingly, while inside the capacitor it depends on the rotation axis location, the external $\boldsymbol{B}^{(1)}$ is uniform and carries
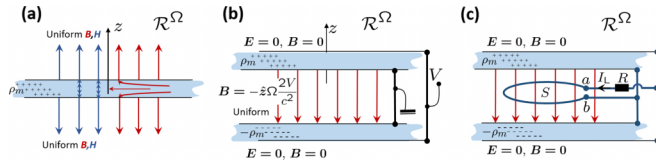
FIG. 3. The leading **B** field in electric and magnetic capacitors, and the rotation-induced memristor. (a) The electric capacitor $\boldsymbol{H}^{(1)}$ (blue) and $\boldsymbol{B}^{(1)}$ (red) fields. They are symmetric around $\hat{z}$. A fictitious magnetic charge density $\rho_m = 2\Omega V/(dc^2)$ resides between the plates. (b) The magnetic capacitor, consisting of two electric capacitors with inverted voltages. This structure can function as a memristor. (c) A resonant structure consisting of a magnetic capacitor and loop.

no information about the axis location. The leading orders of H and B are shown in Fig. 3(a).

2. Rotation-induced magnetic capacitor and memristor

The uniformity of $\boldsymbol{B}^{(1)}$ in the external domain of the parallel plate electric capacitor suggests that it can be used to form a magnetic capacitor for fictitious magnetic charge densities $\pm\rho_m = \pm2\Omega V/(dc^2)$, as shown in Fig. 3(b). Two parallel plate electric capacitors are situated normal to $\hat{z}$ and parallel to each other and are connected to the source and Earth in inverted polarities. Electrically, these two capacitors are connected in parallel. The fields external to the structure mutually cancel and are doubled in the domain between the capacitors, yielding $\boldsymbol{B} = -\hat{z}\Omega\, 2V/c^2$. This device generates magnetic field that is proportional to the electric *voltage* V, as opposed to $\boldsymbol{B}$ in conventional inductors, which is proportional to the electric *current*, thus suggesting a potentially different circuit functionality. This functionality resembles the *memristor* [22,23], a device that generates magnetic flux β due to electric charge q, with *memristance* $M \equiv \beta/q$. Here $q = V2C = V2\epsilon A/d$, and $\beta = A\Omega\hat{z} \cdot \boldsymbol{B}^{(1)}$, yielding $M = \Omega d/(c^2\epsilon)$. Note that epsilon near zero (ENZ) metamaterials [18] at the specific operation frequency ω can be used to increase M. Traditional memristor implementations are nonlinear and active [23]. Here it is a linear passive device in $\mathcal{R}^\Omega$, with energy provided by rotation. Interestingly, M can be positive or negative depending on the rotation direction.

This magnetic capacitor can resonate with a coupled inductor as a special case of the system discussed in Sec. III A. The example shown in Fig. 3(c) is studied in the Supplemental Material [27]. The general expression for the eigenfrequencies in Eq. (18) holds with the substitution $F = Sc^{-2}$ (see the Supplemental Material [27]).

3. Magnetic inductors and rotation-induced electric capacitor

This example, shown in Fig. 4, is the dual structure of the capacitor-inductor system in Secs. III B 1 and III B 2. A conventional inductor is shown in Fig. 4(a). Clearly, $\boldsymbol{E}^{(0)} = \boldsymbol{0}$ everywhere. Neglecting the edge effect (for $h \gg \ell, d$), the $\mathcal{R}^0$ magnetic field is $\boldsymbol{H}^{(0)} = \hat{z}I_L/h$ inside the inductor, and it vanishes outside. Thus, in the $\mathcal{R}^\Omega$ problem, a fictitious electric charge whose leading term is $\rho_e = \Omega\rho_e^{(1)}$, with $\rho_e^{(1)} = 2I_L/(hc^2)$, is generated inside the inductor. Then $\boldsymbol{E}^{(1)} =$
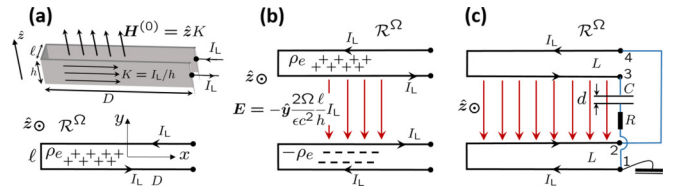

FIG. 4. The leading rotation-induced fields in the inductor-capacitor system. (a) Three-dimensional view of a conventional inductor in $\mathcal{R}^0$ (top) and a top view in $\mathcal{R}^\Omega$ (bottom). A fictitious rotation-induced electric charge exists inside the inductor. (b) Two inductors create a rotation-induced electric capacitor with uniform electric field. (c) A resonant structure.

$\hat{\boldsymbol{y}}\epsilon^{-1}\rho_e^{(1)}y$ inside the inductor, and $\boldsymbol{E}^{(1)} = \text{sgn}\{y\}\hat{\boldsymbol{y}}(2\epsilon)^{-1}\rho_e^{(1)}\ell$ outside the inductor (we neglect edges). If two inductors are placed in parallel with current directions as shown in Fig. 4(b), then the electric fields outside the structure mutually cancel and vanish, while $\boldsymbol{E} = -\hat{\boldsymbol{y}}2\Omega\ell(\epsilon c^2 h)^{-1}I_L$ between the inductors. Thus, a rotation-induced electric capacitor is created between the two inductors. The electric field inside this device is proportional to the electric *current* I_L, as opposed to a conventional capacitor in which $\boldsymbol{E}$ is proportional to the voltage, thus suggesting a potentially different circuit functionality that can be viewed as the dual of the rotation-induced memristor discussed in Sec. III B 2.

The LC circuit shown in Fig. 4(c) consists of an additional "true" capacitor C, possesses the eigenfrequencies given in Eq. (18), with $F = A(\ell/h)c^{-2}$, where A is the capacitor plate area (see the Supplemental Material [27]).

4. The core-shell structure

Here we study the structure shown in Fig. 5. It can be viewed as a natural way to connect the two plate systems in Fig. 3(b), thus enclosing the structure into a finite-size one that allows for a more accurate calculation and control of the leading fields. The inner and outer spherical shells are made of an ideal conductor, have radii a and $b = a + d$, and are held at the potentials $-V_0$ and 0, respectively. The corresponding $\mathcal{R}^0$ problem is shown in Fig. 5(a). Since Eqs. (6a)–(8c) are independent of the rotation axis, we conveniently solve the leading field terms in the coordinate systems $\mathcal{R}_c^0, \mathcal{R}_c^\Omega = (x_c, y_c, z)$ and (r_c, θ_c, ϕ_c), whose origin coincides with the shell's center and which have the same z axis as $\mathcal{R}^0$ and $\mathcal{R}^\Omega$. We divide the space into three domains, defined conveniently in $\mathcal{R}_c^0$ and $\mathcal{R}_c^\Omega$ as $\mathcal{D}_i$, $i = 1, 2, 3$, for $r_c < a$, $a \leqslant r_c \leqslant b$, and $r_c > b$, respectively. $\mathcal{D}_i$ is filled by a material with ϵ_i and μ_i. The $\mathcal{R}^0$ fields, written in $\mathcal{R}_c^0$, are

$$\boldsymbol{E}_1^{(0)} = \boldsymbol{E}_3^{(0)} = \boldsymbol{0}, \quad \boldsymbol{E}_2^{(0)} = -\hat{\boldsymbol{r}}_c V_0 \frac{ab}{dr_c^2}, \quad \boldsymbol{H}^{(0)} = \boldsymbol{0} \; \forall \boldsymbol{r}. \quad (20)$$

From Eq. (8c) the rotation-induced fictitious magnetic charge in $\mathcal{D}_i$ is given by $\rho_{m,i} = \Omega\rho_{m,i}^{(1)}$, $i = 1, 2, 3$, with

$$\rho_{m,1}^{(1)} = \rho_{m,3}^{(1)} = 0, \quad \rho_{m,2}^{(1)} = -V_0 A \frac{\cos\theta_c}{r_c^2}, \quad A = \frac{2ab}{\mu_2 c^2 d}, \quad (21)$$
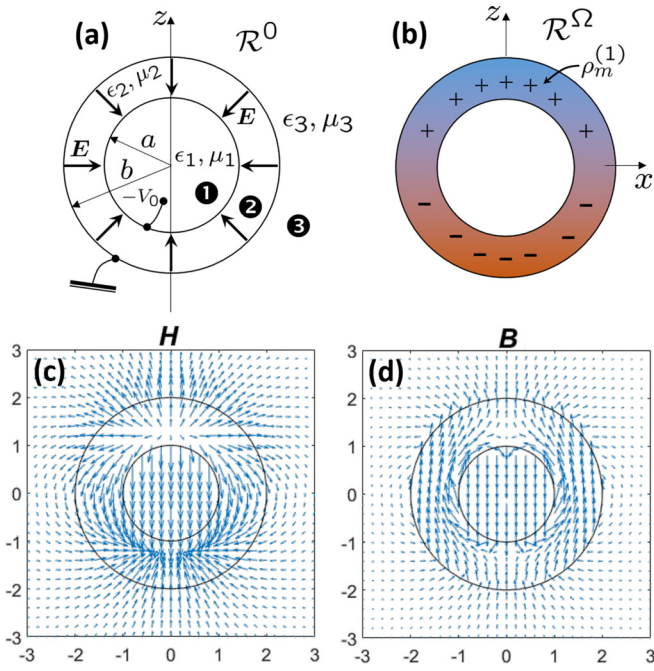
FIG. 5. The core-shell structure. (a) The $\mathcal{R}^0$ problem. (b) The rotation-induced fictitious magnetic charge $\rho_m^{(1)}$. (c) $\boldsymbol{H}^{(1)}$ and (d) $\boldsymbol{B}^{(1)}$ for $a = 1$ m, $b = 2$ m, and $\mu_1 = \mu_2 = \mu_3 = \mu_0$ (arbitrary scale). $\boldsymbol{H}_{1,2,3}^{(1)}$ and $\boldsymbol{B}_{1,3}^{(1)}$ are *independent* of the rotation axis location. Only $\boldsymbol{B}_2^{(1)}$ (in $\mathcal{D}_2 : a \leqslant r \leqslant b$) depends on the rotation axis, which here is centered at the sphere.

as shown in Fig. 5(b). The first-order Φ_m in $\mathcal{D}_i$ satisfy Eq. (8c) with $n = 1$. They are expressed as the spherical harmonics

$$\Phi_{m,1}^{(1)} = V_0 C_1 r_c \cos \theta_c = V_0 C_1 z, \tag{22a}$$

$$\Phi_{m,2}^{(1)} = V_0 \left(C_2 r_c + D_2 r_c^{-2} \right) \cos \theta_c + V_0 (A/2) \cos \theta_c, \tag{22b}$$

$$\Phi_{m,3}^{(1)} = V_0 D_3 r_c^{-2} \cos \theta_c. \tag{22c}$$

The last term in Eq. (22b) is a particular solution that accounts for the source term $\rho_{m,2}^{(1)}$. The yet unknown coefficients $C_1, C_2, D_2,$ and D_3 are determined by imposing continuity on the tangential $\boldsymbol{H}^{(1)} = -\nabla \Phi_m^{(1)}$ (no electric currents yet) and normal $\boldsymbol{B}^{(1)}$. We note that these magnetic fields are solely rotation-induced fields; thus, they are not repelled by the perfect electric conductor (PEC) shells (see Sec. II and the discussion pertaining to Fig. 1).

Since $\boldsymbol{E}_{1,3}^{(0)} = \boldsymbol{0}$ [see Eq. (20)], we have

$$\boldsymbol{B}_k^{(1)} = \mu_k \boldsymbol{H}_k^{(1)}, \quad k = 1, 3. \tag{23}$$

Regarding $\boldsymbol{B}_2^{(1)}$, note that from Eq. (9b) and from $\boldsymbol{E}_2^{(0)}$ in Eq. (20) this field formally depends on ρ. Nevertheless, this dependence does not survive the continuity conditions for normal $\boldsymbol{B}$, which is evident from Eq. (4b) (see details in the Supplemental Material [27]). As a result $C_1, C_2, D_2,$ and D_3 are independent of the rotation axis and, consequently, the same holds for the fields $\boldsymbol{H}_\ell^{(1)}$, $\ell = 1, 2, 3$, and $\boldsymbol{B}_{1,2}^{(1)}$. By imposing the continuity conditions as discussed above we obtain a set of linear equations for the unknown coefficients that can be solved analytically. See the Supplemental Material [27] for details and for explicit expressions of the coefficients for
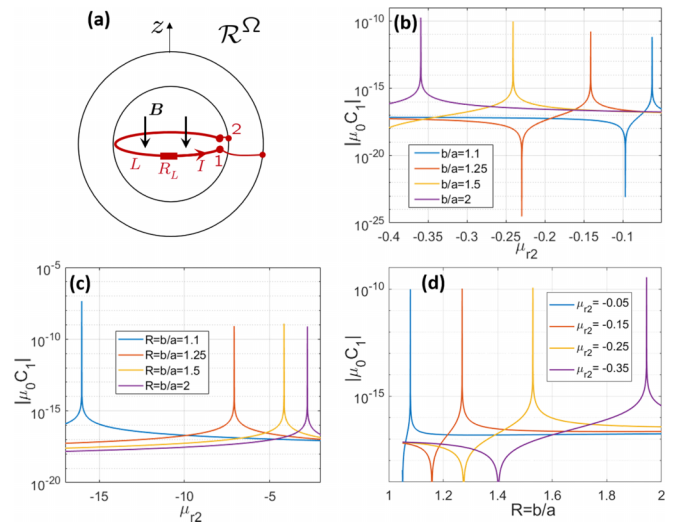

FIG. 6. The resonating core-shell structure. (a) An inductor L is inserted in $\mathcal{D}_1$ with ports connected to the inner and outer shells. (b) $|\mu_0 C_1| = 2F/S$ vs μ_{r2} for various values of $u = b/a$. (c) The same as (b), but for a different domain of μ_{r2}. (d) $|\mu_0 C_1| = 2F/S$ vs $u = b/a$ for various values of μ_{r2}.

arbitrary ϵ_i and μ_i. Note that $\boldsymbol{B}_1^{(1)} = -\mu_1 C_1 \hat{\boldsymbol{z}}$ is uniform. It can be increased by tuning μ_2 such that C_1 becomes singular. For $\mu_1 = \mu_3 = \mu_0$ unbounded C_1 can be achieved with moderate $\mu_{r2} < 0$ (see the Supplemental Material [27]). The structures for $\boldsymbol{H}^{(1)}$ and $\boldsymbol{B}^{(1)}$ are shown in Figs. 5(c) and 5(d).

The core-shell structure may exhibit rotation-induced gain by letting the rotation-induced $\boldsymbol{B}^{(1)}$ generate flux inside an inductor. A possible configuration is shown in Fig. 6(a). An inductor with inductance L is inserted into $\mathcal{D}_1$, with the cross section normal to $\hat{\boldsymbol{z}}$. The resistor R_L represents the system's Ohmic loss. Note the polarity of the coil-shell connection with respect to rotation. By following essentially the same analysis as in Sec. III B 2, we obtain Eq. (18) for the eigenfrequencies, where $\omega_0 = (LC_s)^{-1/2}$; $C_s = 4\pi \epsilon_2 ab/d$ is the double-shell capacitance in $\mathcal{R}^0$; $\tau = (R_L + R_r) C_s$, with R_r being the radiation resistance; and $F = \mu_1 C_1 S/2$, where S is the inductor area; see the Supplemental Material [27] for details. Figures 6(b) and 6(c) present $\mu_1 C_1$ for $\mu_1 = \mu_3 = \mu_0$ vs μ_{r2} and $u = b/a$. C_1 is unbounded at the $\mu_{r2} < 0$ values given by Eq. 20(b) in the Supplemental Material [27].

Recall that while F is extremely small, due to the ω_0^2 multiplication in the imaginary part of Eq. (18) F needs to be only marginally larger than τ to produce observable gain. We perform a preliminary parametric study of the complex eigenfrequency. Note that $[\text{Im}(\omega_{1,2})]^{-1}$ is the characteristic rise (decay) time of the rotation-induced gain (loss). Figure 7 shows $\text{Im}\{\omega_{1,2}\}$ vs $u = b/a$ for various values of a for $\mu_{r2} = -0.35$ and $\mu_{r1} = \mu_{r3} = \epsilon_{r2} = 1$. Within this range of parameters $\text{Re}\{\omega_{1,2}\}$ is on the order of 1–20 MHz and is provided in the Supplemental Material [27]. Calculations are performed for Earth rotation rate $\Omega = 7.2722 \times 10^{-5}$ (very similar to Mars's) and for $\Omega = 0.1$. In all cases the inductor L consists of a loop with $N = 10$ turns of a thin wire whose diameter is 0.2 mm, and the loop radius is 0.75 times the inner shell radius. We used standard expressions for the self-inductance of thin wire loops available in the literature [17].
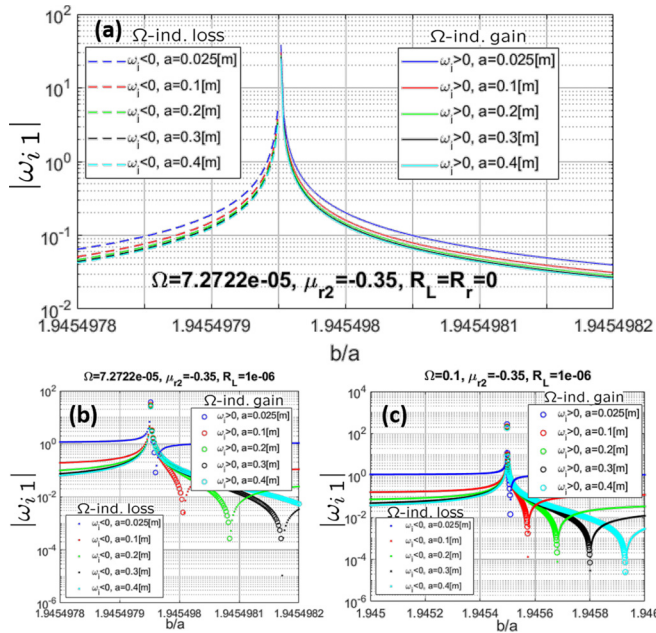
FIG. 7. The imaginary part of the complex eigenfrequency, $\omega_i = \text{Im}\{\omega_{1,2}\}$. (a) $|\omega_i|$ in log scale, with no loss ($R = 0$), for the Earth rotation rate ($\Omega = 7.2722 \times 10^{-5}$). (b) $|\omega_i|$ with $R = R_L + R_r = 10^{-6}$ and for the Earth rotation rate. Gain, corresponding to $\text{Im}\{\omega\} > 0$, is shown by circles. It is obtained whenever $-\sigma\Omega F > \tau/2$. Loss ($\text{Im}\{\omega\} < 0$) is shown by dots. Peak values are higher than those seen in the plot but below the scan resolution. (c) The same as (b), but for $\Omega = 0.1$, resulting in a nearly 3 orders of magnitude increase in gain and b/a bandwidth.

We assume $R_L = 0$ in Fig. 7(a) and $R_L = 10^{-6}$ Ω in Figs. 7(b) and 7(c), corresponding to superconductors and exceptionally high-quality conductors. In all calculations we set the total resistance to $R = R_L + R_r$, where the radiation resistance R_r is estimated with the standard expression provided in the Supplemental Material [27] (see details there). The specific values of R_r vary as a function of a and b, but in all the cases shown it is on the order of 10^{-5} Ω.

IV. CONCLUSIONS

We have developed a systematic framework governing the ED of rotating electrical circuits and systems in their rest frame of reference $\mathcal{R}^\Omega$. Rotation-induced effects such as fictitious magnetic and electric charges and gain and instabilities were reported. These effects may pave the way for various circuit devices such as magnetic capacitors with fictitious magnetic charge in which the charge and the associated **H** field are proportional to the device voltage, and electric capacitors with fictitious electric charge in which the latter and the associated **E** field are proportional to the device current. The rotation-induced fictitious charges are proportional to the rotation rate Ω. These effects lead to new implementations of memristors with positive or even negative memristance and their dualities. A Poynting theorem in $\mathcal{R}^\Omega$ was derived, and it was shown that a power exchange between the rotating platform and the electric circuit is possible in $\mathcal{R}^\Omega$. Gain and instabilities induced by rotation were studied in a general setting of LC circuits, and several specific examples were provided. The rotation-induced gain and loss are manifestations of the aforementioned power exchange laws. These findings may pave the way to new materials, circuits, and energy harvesting technologies.

Finally, we note that rest-frame analysis of acoustic and elastic waves in rotating bulk materials was developed and studied for several decades, essentially in the context of geophysics (see, e.g., [34–36]). The interest there is focused on the effect of rotation on wave trajectories and polarization for geophysical remote sensing applications. This class of problems is fundamentally different from electromagnetic problems since they can exist only inside materials, and the material mechanics plays a pivotal role. Centripetal and Coriolis forces affect the wave dynamics. The passage to rest-frame quasistatic acoustics or elasticity theory of rotating systems may find application in the field of acoustic metamaterials, which consist of small mechanical inclusions [37,38]. While the acoustic equivalent of negative-index EM metamaterials and the corresponding circuit elementlike building blocks have been explored, the effect of rotation on the rest-frame acoustic and elastic constitutive relations in this regime of parameters still needs to be studied.

[1] S. Ezekiel and H. J. Arditty, *Fiber-Optic Rotation Sensors*, Springer Series in Optical Sciences (Springer, Berlin, 1982).

[2] H. J. Arditty and H. C. Lefevre, Sagnac effect in fiber gyroscopes, Opt. Lett. **6**, 401 (1981).

[3] H. C. Lefevre, Fundamentals of the interferometric fiber-optic gyroscope, Opt. Rev. **4**, 20 (1997).

[4] E. J. Post, Sagnac effect, Rev. Mod. Phys. **39**, 475 (1967).

[5] B. Z. Steinberg, Rotating photonic crystals: A medium for compact optical gyroscopes, Phys. Rev. E **71**, 056621 (2005).

[6] B. Z. Steinberg and A. Boag, Splitting of micro-cavity degenerate modes in rotating photonic crystals - The miniature optical gyroscopes, J. Opt. Soc. Am. B **24**, 142 (2007).

[7] B. Z. Steinberg, J. Scheuer, and A. Boag, Rotation induced super structure in slow-light waveguides with mode degeneracy: Optical gyroscopes with exponential sensitivity, J. Opt. Soc. Am. B **24**, 1216 (2007).

[8] S. Sunada and T. Harayama, Sagnac effect in resonant microcavities, Phys. Rev. A **74**, 021801(R) (2006).

[9] S. Sunada and T. Harayama, Design of resonant microcavities: Application to optical gyroscopes, Opt. Express **15**, 16245 (2007).

[10] L. Ge, R. Sarma, and H. Cao, Rotation-induced mode coupling in open wavelength-scale microcavities, Phys. Rev. A **90**, 013809 (2014).

[11] R. Sarma, L. Ge, J. Wiersig, and H. Cao, Rotating Optical Microcavities with Broken Chiral Symmetry, Phys. Rev. Lett. **114**, 053903 (2015).

[12] R. Sarma, L. Ge, and H. Cao, Optical resonances in rotating dielectric microcavities of deformed shape, J. Opt. Soc. Am. B **32**, 1736 (2015).

[13] Y. Mazor and B. Z. Steinberg, Rest Frame Interference in Rotating Structures and Metamaterials, Phys. Rev. Lett. **123**, 243204 (2019).

[14] B. D. Newsom, Habitability factors in rotating space station, Space Life Sci. **3**, 192 (1972).

[15] G. R. Clement, A. P. Bukley, and W. H. Paloski, Artificial gravity as a countermeasure for mitigating physiological conditioning during long-duration space missions, Front. Syst. Neurosci. **9**, 92 (2015).

[16] K. N. Bretl and T. K. Clarck, Improved feasibility of astronaut short-radius artificial gravity through a 50-day incremental, personalized, vestibular acclimation protocol, npj Microgr. **6**, 22 (2020).

[17] S. Tretyakov, *Analytic Modeling in Applied Electromagnetics* (Artech House, Boston, 2003).

[18] *Metamaterial: Physics and Engineering Explorations*, edited by N. Engheta and R. W. Ziolkowski (IEEE Press, Piscataway, NJ, 2006).

[19] B. D. H. Tellegen, The gyrator, a new electric network element, Philips Res. Rep. **3**, 81 (1948).

[20] X.-L. Qi, T. L. Hughes, and S.-C. Zhang, Topological field theory of time-reversal invariant insulators, Phys. Rev. B **78**, 195424 (2008).

[21] X.-L. Qi, R. Li, J. Zang, and S.-C. Zhang, Inducing a magnetic monopole with topological surface states, Science **323**, 1184 (2009).

[22] L. O. Chua, Memristor–The missing circuit element, IEEE Trans. Circuit Theory **18**, 507 (1971).

[23] D. B. Strukov, G. S. Snider, D. R. Stewart, and R. S. Williams, The missing memristor found, Nature (London) **453**, 80 (2008).

[24] C. W. Misner, K. S. Thorne, and J. A. Wheeler, *Gravitation* (Princeton University Press, Princeton, NJ, 2017).

[25] T. Shiozawa, Phenomenological and electron-theoretical study of the electrodynamics of rotating systems, Proc. IEEE **61**, 1694 (1973).

[26] J. L. Anderson and J. W. Ryon, Electromagnetic radiation in accelerated systems, Phys. Rev. **181**, 1765 (1969).

[27] See Supplemental Material at http://link.aps.org/supplemental/10.1103/PhysRevB.107.195418 for derivations of the rest frame quasistatic theory and analytic details of the examples.

[28] F. London, *Superfluids* (Dover, New York, 1961), Vol. 1.

[29] J. E. Hirsch, The London moment: What a rotating superconductor reveals about superconductivity, Phys. Scr. **89**, 015806 (2014).

[30] A. F. Hildebrandt, Magnetic Field of a Rotating Superconductor, Phys. Rev. Lett. **12**, 190 (1964).

[31] M. Born and E. Wolf, *Principles of Optics*, 6th ed. (Pergamon Press, Oxford, 1980).

[32] J. D. Jackson, *Classical Electrodynamics*, 2nd ed. (Wiley, New York, 1975).

[33] C. A. Balanis, *Antenna Theory: Analysis and Design*, 3rd ed. (Wiley, Hoboken, NJ, 2005).

[34] M. Schoenberg and D. Censor, Elastic waves in rotating media, Q. Appl. Math. **31**, 115 (1973).

[35] R. Snieder, C. Sens-Schönfelder, E. Ruigrok, and K. Shiomi, Seismic shear waves as foucault pendulum, Geophys. Res. Lett. **43**, 2576 (2016).

[36] Y. Durukan, M. Shevelko, A. Peregudov, E. Popkova, and S. Shevchenko, The effect of a rotating medium on bulk acoustic wave polarization: From theoretical considerations to perspective angular motion sensor design, Sensors **20**, 2487 (2020).

[37] Y. Ding, Z. Liu, C. Qiu, and J. Shi, Metamaterial with Simultaneously Negative Bulk Modulus and Mass Density, Phys. Rev. Lett. **99**, 093904 (2007).

[38] S. Zhang, L. Yin, and N. Fang, Focusing Ultrasound with an Acoustic Metamaterial Network, Phys. Rev. Lett. **102**, 194301 (2009).